Application of Static Charge Dissipation to Mitigate Electric Discharge Bearing Currents

Annette Muetze, *Member, IEEE*, and H. William Oh, *Member, IEEE*

***Abstract*—Today, the physical cause-and-effect chains of inverter-induced high-frequency bearing currents have been well understood, but little has been known on not only theoretically possible, but also cost-effective mitigation techniques for a certain drive configuration. This paper focuses on the mitigation of discharge bearing currents, which occur predominantly with smaller motors of up to several kilowatts. We present a new mitigation technique where any voltage build-up across the bearing is discharged via static charge dissipation through a parallel path before an electric breakdown inside the bearing occurs. The technique is based on the field emission effect, has ultralow friction and negligible wear, and is very robust toward contamination, when compared with conventional carbon-based brushes.**

***Index Terms*—Bearings (mechanical), common-mode voltage, electric breakdown, electric field effects, variable-speed drives.**

NOMENCLATURE

BVR	Bearing voltage ratio.
CM	Common-mode.
DE	Drive-end.
EDM	Electric discharge machining.
ESD	Electrostatic discharge.
F-N	Fowler–Nordheim.
HVAC	Heating, ventilation, airconditioning.
NDE	Nondrive-end.
VFD	Variable-frequency drive.
a	Constant.
b	Constant.
d	Gap spacing.
p	Pressure.
v_{bea}	Voltage across the bearing.
v_{com}	Common-mode voltage.
A_{c}	Cross-sectional area.
C_{wr}	Capacitance between stator-winding and rotor.
I	Current.
E	Electric field-strength.
E_{m}	Microscopic electric field-strength at the microscopic surface of the contact.
R_{f}	Resistance between the two poles of the microfiber brush.
V	Voltage.
V_{B}	Breakdown voltage.
β	Total electric field enhancement factor.
β_{g}	Geometric electric field enhancement factor.
β_{m}	Microscopic electric field enhancement factor.
ρ	Pressure-gap product.

Paper IPCSD-07-060, presented at the 2007 IEEE International Electric Machines and Drives Conference, Antalya, Turkey, May 3–5, and approved for publication in the IEEE TRANSACTIONS ON INDUSTRY APPLICATIONS by the Industrial Drives Committee of the IEEE Industry Applications Society. Manuscript submitted for review May 8, 2007 and released for publication July 26, 2007.

A. Muetze is with the School of Engineering, University of Warwick, Coventry CV4 7AL, U.K. (e-mail: a.muetze@warwick.ac.uk).

H. W. Oh is with Electro Static Technology, Mechanic Falls, ME 04256 USA (e-mail: hwoh@est-static.com).

Color versions of one or more of the figures in this paper are available online at http://ieeexplore.ieee.org.

Digital Object Identifier 10.1109/TIA.2007.912758

I. INTRODUCTION

INVERTER-INDUCED high-frequency bearing currents are a parasitic effect that can occur in variable-speed drive systems. Different types of bearing currents that have different cause-and-effect chains can be distinguished. With the advent of modern drive technology, these phenomena have been well recognized and physical explanations have been given [1]–[15]. While the cause-and-effect chains have been understood, little has still been published not only on theoretically possible, but also on cost-effective mitigation techniques for a certain drive configuration.

Among the different bearing current types that have been identified, this paper focuses on the mitigation of high-frequency discharge bearing currents [also "electric discharge machining (EDM)-bearing currents"]. These occur predominantly with smaller motors of up to several kilowatts [14], [15]. Common mitigation techniques are common-mode (CM) voltage filters, hybrid/ceramic bearings, and—sometimes—brushes.

We present a new mitigation technique that is based on static charge dissipation. Here, any voltage build-up across the bearing is discharged due to the electric field emission effect through a parallel path before an electric breakdown inside the bearing occurs. The technique has ultralow friction and negligible wear, and is very robust toward contamination, when compared to conventional carbon-based brushes. It is also easy to install and cost-effective.

The paper is organized as follows: First, a brief review of EDM-bearing currents is given in Section II. Then, the principle idea of the presented mitigation technique is presented in Section III, followed by a brief summary of the required background information of electrostatic discharge (ESD) effects in Section IV. In the main part of the paper, the theory of the proposed technique is discussed (Section V) and experimental results are presented (Section VI). Conclusions are drawn at the end of the paper in Section VII.

II. REVIEW: DISCHARGE BEARING CURRENTS

A. Physical Cause-and-Effect Chain

If no additional measures, like special filters or control schemes, are applied, a voltage-source inverter presents a voltage-source in the CM circuit. The generated CM voltage

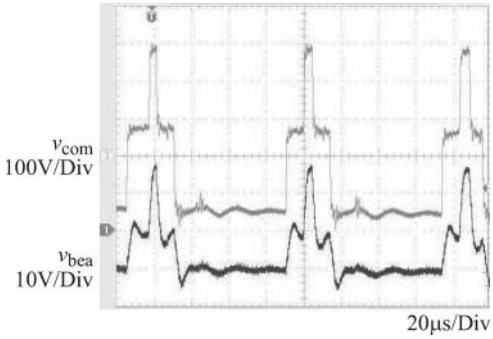

Fig. 1. At electrically insulating lubrication film, the voltage across the bearing (v_{bea}) mirrors the CM voltage (v_{com}); squirrel-cage induction motor, 215 TC frame, 10 hp rated power, motor speed 1800 r/min.

TABLE I
RANGES OF THE VOLTAGE ACROSS THE BEARING

Supply voltage (3ph) (line-to-line, rms) V	Inverter dc-link voltage*) V	Peak CM voltage**) V	Voltage across bearing (BVR = 0.01...0.1)***) V
200	270	180	1.8...18
240	324	216	2.2...22
380	513	342	3.4...34
460	621	414	4.1...41

*) $V_{dc} = \frac{3}{\pi}\sqrt{2}V_{LL,rms,1}$; **) $v_{com,pk} = \frac{2}{3}V_{dc}$; ***) $v_{bea,pk} = BVR \cdot v_{com,pk}$

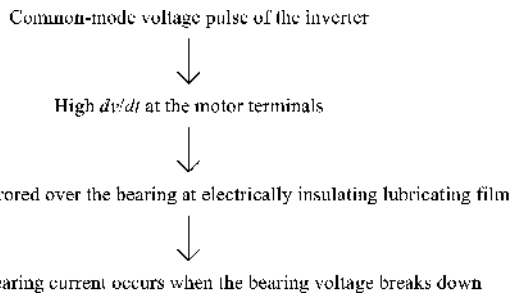

Fig. 2. Phycial cause-and-effect chain of EDM-bearing currents.

contains high-frequency components that interact with capacitances inside the machine that have not been of influence at line operation. As a result, at electrically insulating ("intact") lubrication film, the voltage across the bearing v_{bea} mirrors the CM voltage v_{com} (Fig. 1). The voltage across the bearing is also frequently referred to as "shaft voltage." It should be noted that the voltage *across* the bearing has a very different nature than the "shaft" voltage *along* the shaft that can be generated by high-frequency CM currents.

The capacitive voltage divider between v_{bea} and v_{com} is commonly referred to as "bearing voltage ratio" (BVR) (e.g. [4], [5]). The BVR is typically in the order of several percent, with an upper bound of 10% for "typical" machines [16].

Table 1 gives an overview of the ranges of the maximum voltage across the bearing for different 3 ph supply voltages and BVR = 1–10%. Increased voltage at the motor terminals due to voltage reflection can increase these values additionally.

When a breakdown of the electrically loaded oil film between the rolling elements and the running surface takes place, a discharge bearing current pulse occurs (Figs. 2 and 3).

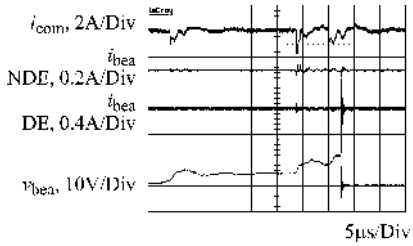

Fig. 3. Measured discharge bearing current; induction motor, frame size 160 mm, 11 kW rated power, motor speed 1500 r/min, bearing temperature ≈30°C [14]; i_{com}: stator CM current; i_{bea}, bearing current; NDE, nondrive-end; DE, drive-end. The voltage across the bearing changes with every switching instant (occurrence of a stator-winding CM current, traces 1 and 4), the discharge bearing-current, however, occurs independently of the switching instant and mostly in one of the bearings (traces 2 and 3).

Depending on the operating conditions of the machine, the threshold voltage for a breakdown to occur is approximately 5–30 V, where the occurrence of the breakdowns itself is a statistically distributed effect [14]. A comparison with Table I shows that the voltage across the bearing at electrically insulating lubricating film can easily exceed the threshold voltage.

A lot of the literature referred to in the following has been taken from the context of electrostatic discharging and electric breakdown of microelectronic devices. Therefore, we would like to emphasize that the charging mechanism of the bearings as described is fundamentally different from the "triboelectric" charging by separation. As opposed to the capacitively coupled charging of the bearing, the triboelectric charging occurs when two materials with different electron affinity that have been in contact are separated. The degree to which the charge stays on the materials depends mostly on their conductivities and initial charge densities [17].

B. Common Mitigation Techniques

Commonly, one of the following mitigation techniques for discharge bearing currents are used with commercial applications.

1) *CM voltage filters* are complex circuits that are designed to reduce or eliminate the CM voltage, notably its high-frequency components. The filters are a rather costly addition to the drive system. Often, they are applied to attenuate electromagnetic noise, and then, are combined with differential noise filters. It should be mentioned that, on the academic level, comparatively a lot is known about the design of special modulation techniques and inverter-output filters to eliminate the CM voltage.
2) *Carbon brushes* use electrically conductive carbon graphite and provide an electrical connection between the motor shaft and the frame parallel to the bearing. A graphite film deposits on the contact area during sliding. Humidity creates a water layer on the graphite, thereby rendering the brushes self-lubricating. Commonly quoted problems are excessive wear and hot-spotting/thermal moulding as the contact is transferred to fewer, expanded, more fragile spots during the sliding, as well as brush dusting/low-humidity lubrication [18]. Maintaining good electrical contact at the high frequencies of the CM

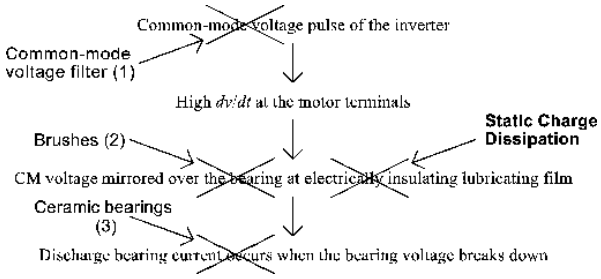

Fig. 4. Points of impact of different mitigation techniques on the EDM-bearing current physical cause-and-effect chain.

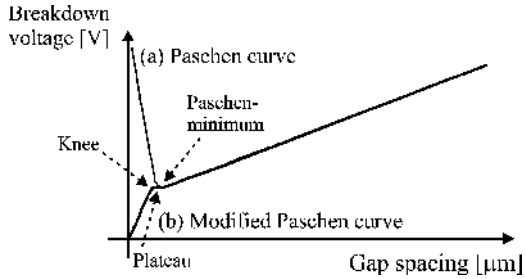

Fig. 5. Qualitative sketch. (a) Paschen curve. (b) Modified Paschen curve based on [25].

voltage poses additional challenges on the brush design and installation.

3) *Hybrid/full ceramic bearings* have ceramic (silicon nitride) rolling elements and quality (alloy or carbon) steel races or both ceramic rolling elements and races, respectively. Thereby, they introduce a large insulating gap into the bearing and prevent electric discharge in the bearing. However, the charges on the rotor seek an alternate path to the ground, typically through the attached equipment if the rotor is not isolated. Irrespective of bearing currents, ceramic bearings are mostly selected for mechanical reasons. These bearings are significantly more expensive than conventional steel bearings. In addition, because ceramic bearings and steel bearings differ in compressive strength, ceramic bearings must be resized in most cases to handle mechanical static and dynamic loadings.

The points of impact of these mitigation techniques on the EDM-bearing current physical cause-and-effect chain are illustrated in Fig. 4.

III. Principle Idea of the Proposed Mitigation Technique

The proposed mitigation technique has the same point of impact as brushes do, that is, it prevents the voltage build-up across the bearings (Fig. 4). However, in contrast to the spring-loaded mechanism of conventional carbon brushes, the technique has ultralow fricition and negligible wear, and is relatively robust toward contamination, and thus, it is free of the problems that are commonly quoted with brushes (Section II-B). The electric contact between the motor frame and the shaft is established using the electric field emission effect. In order to understand this technique, it is important to well distinguish between the different ESD mechanisms and their associated length scales of the gaps. In the next section, we first provide an overview of this topic to help the reader understand the "overall picture" (Sections IV-A through IV-D), and give a summary of the key values (Section IV-E) that we use in the discussion of further details of the proposed new mitigation technique (Section V).

IV. Background on Electrostatic Discharge Mechanisms

A. Electric Contact Without Mechanical Contact

In order to understand the mitigation technique for EDM-currents presented in this paper, it is important to be aware of the fact that "electric contact" does not necessarily also mean "mechanical contact." In this section, we explain some mechanisms to achieve the electric contact without having any mechanical contact. To this aim, we first review the three main prebreakdown current mechanisms and lengths scales (Sections IV-B–IV-D).

B. Gaseous Discharge for "Large" Gaps (Above ≈5 μm)

Gaseous breakdown at "large" gaps is commonly described using the Paschen curve that is based on Paschen's law [19]. The Paschen curve correlates the breakdown voltage V_{B} and the reduced variable $\rho = pd$, where p is the pressure and d is the gap spacing. For each pressure–gap product, it predicts a minimum breakdown voltage, the so-called Paschen-minimum (Fig. 5).

The underlying understanding of the breakdown mechanism is the Townsend (avalanche) breakdown in gases. That is, the cascading effect of secondary electrons obtained by collisions and impact ionization of the gas ions accelerating across the gap [20], [21]. The breakdown voltage is affected by the geometrical configuration of a discharge gap, particularly the shape and the size of the electrodes used in the tests [22], [23].

The Paschen curve is well known. Breakdown for gaps greater than approximately 10 μm has been well studied, and the breakdown limit for air at one atmosphere is identified as 3 V/μm (3 kV/mm). The minimum breakdown voltage is approximately 360 V and occurs at a gap spacing of 5 μm, and it *increases* for smaller gaps [24]. The misconception that the same breakdown mechanism would hold for smaller gap spacings is best illustrated quoting [24]:

> While the left, rising part of the Paschen curve *can* be observed at low pressure and large gap spacing, it is not observed for air gaps at atmospheric pressure [25]. One proof of this is the 80 V breakdown voltage reported for a 0.12 μm air gap in [26]. Nevertheless, there exists a widespread misconception that there exists a minimum breakdown voltage for air gaps and that if the spacing of a device is scaled-down below ≈ 5 μm, then breakdown will not occur.

C. Electric Field Emission for "Small" Gaps (≈ 5 nm to ≈5 μm)

Field emission is a form of quantum tunneling and is also known as Fowler–Nordheim (F–N) tunneling [27]–[29]. It is the process whereby electrons tunnel through a barrier in the presence of a high electric field (that is often associated with a deformed surface potential barrier). The potential at which the

electrons have sufficient kinetic energy to do so is commonly referred to as barrier gap or work function potential. As the kinetic energy of the charge carriers has a certain distribution over the population, some of them have enough energy to cross the gap even much below the breakdown voltage.

In contrast to the Frenkel–Powl tunneling commonly used for semiconductor devices, the F–N tunneling does not rely on defects in a material.

The F–N equation relates the current (or the current density) before breakdown and the electric field or voltage. The simplified form is shown as [30]

$$I = aV^2 \exp\left(-\frac{\mathrm{b}}{V}\right) \tag{1}$$

where I is the field emission current, V is the voltage, and a and b are constants that contain, among others, the emitting area, work function, a field enhancement factor (see later), and functions of the electric field and the work function that are approximated as constants.

The plot of $1/E$ versus $\ln(I/E^2)$ [or $1/V$ versus $\ln(I/V^2)$] is referred to as the F–N plot. It allows to verify whether a measured current is due to field emission, in which case a straight line with a negative slope is obtained, where the slope is proportional to the work function of the metal [29].

The field enhancement factor, commonly denoted by β, includes the enhancement of the electric field due to the geometry β_{g}, and due to the microscopic peaks in the (polished!) contact surface β_{m}, and can reach more than two orders of magnitudes [31]. Then,

$$V = d\frac{E_{\mathrm{m}}}{\beta} \tag{2}$$

where E_{m} is the microscopic electric field strength at the microsurface of the contact.

The electrons resulting from field emission can initiate an electric breakdown that occurs when the (local) field emission current density (at microscopic level) exceeds a critical value [31]. This electric breakdown due to the field emission effect occurring at smaller gaps is included in the little-known *modified* Paschen curve [25]. It is best explained by quoting [24] again:

> The modified Paschen curve shows a platform where the pure Paschen curve would have a minimum which is interpreted as the transition region between the gaseous Townsend avalanche and field emission induced breakdown. For smaller gaps (left) of the plateau, breakdown is only due to field emission. The breakdown voltage drops to zero. Details of the geometry and the metal electrode properties influence the exact location of the transition.

D. Tunneling for "Ultrathin" Gaps

This mechanism does not relate directly to the topic of this paper and we are listing it for completion only. As the gap size decreases, the probability of electrons tunneling across an insulating barrier increases. For "ultrathin" gaps ($\approx$2 nm [24]), this can result in a significant tunneling current.

E. Summary of Key Qualitative Results

We are using results published in the context of the microelectronics industry as the starting point for our theoretical investigation [24], [31]–[34]. Though the context of this paper is very different, we will show how these results can be applied to develop a reliable and cost-effective mitigation technique for EDM-bearing currents.

TABLE II
PREBREAKDOWN CURRENT MECHANISMS AND LENGTH SCALES [24]

Current mechanism	Gap distance
Townsend avalanche of gaseous ions	$> 5\mu$m
Field emission of electrons	2nm to 5μm
Tunneling of electrons	$<$ 2nm

Table II shows a summary of the prebreakdown current mechanisms and length scales according to [24] and [32], who draw the following conclusions concerning electric breakdown and ESD phenomena for devices with nanometer-to-micron gaps:

"1) Breakdown is easy across gaps with spacings $<5\ \mu$m and is well below the $\approx$360 V Paschen curve minimum.
2) The prebreakdown current mechanism is field emission.
3) The *modified* Paschen curve that includes field emission effects can be used to predict the breakdown of microdevices."

Similar conclusions have been drawn by the authors of [31]:

"1) For closely spaced contacts in air, Paschen's law is only valid for contact gaps greater than about 6 μm.
2) For contact gaps less than about 4 μm, the breakdown voltage V_{b} in air is a linear function of the contact gap.
3) For contact gaps less than about 4 μm, the electric field at a microprojection . . . to produce a very high current density, field emission electron beam . . . Electrical breakdown between the contact is achieved . . . ."

In the following, we are summarizing some key qualitative results.

1) Metal–air–metal [24]:
   $V_{\mathrm{B}}/d = 156$ V/μm (conservative estimate, neglecting the influence of the curvature and the film); breakdown voltages 151 and 135 V (two samples), 0.9 μm gap; glass deposited on a 100 nm thick chrome and a chrome finger with 2 μm diameter. The modified Paschen curve was obtained for gap spacings between 0.9 μm and 4.0 μm, where the knee was found at 2 μm. The field emission behavior was confirmed via the F–N plot.
2) Metal–air–metal [31]:
   $V_{\mathrm{B}}/d = 110$ V/μm and $V_{\mathrm{B}}/d = 65$ V/μm from data obtained in [33] and [34]; [33]: Fe polished needle with 0.6 mm diameter, 0.05 mm radius, and silver disc, gap spacings 0.2–40 μm; [34]: very carefully developed contact system, clean room measurements, Ni, Al, and brass contacts—no difference in V_{B} was found, showed that Paschen's law is not applicable for gaps between 0 and 4 μm.

V. PROPOSED MITIGATION TECHNIQUE IN THEORY

A. Introduction

With our application, we do not consider ESD as an unwanted, destructive effect, but use the underlying phenomena as a means to discharge the voltage across the bearing v_{bea} through a parallel path. Thereby, we prevent an electric breakdown occurring

inside the bearing that would result in a potentially harmful EDM-bearing current pulse (Fig. 4). By using ESD and the electric field emission effect as mechanisms to provide an electrical contact, we bypass the problems commonly quoted along with mechanical-contact based carbon brushes (Section II-B).

B. Discussion of Orders of Magnitudes and Requirements

The values for v_{bea} shown in Table I (Section II) are far below the Paschen minimum (Section IV-B). Thus, considering only the gaseous, Townsend breakdown mechanism, one would mistakenly draw the wrong conclusion that v_{bea} could not be discharged by ESD through a path parallel to the bearing. However, exploiting the field emission effect, this *can* be achieved successfully.

To this aim, the following requirements must be met:

1) Locally, the electric field strength for a breakdown due to field emission to occur must be achieved.
2) The voltage across the bearing needs to be discharged through the parallel path before an electric breakdown along with a potentially harmful EDM-bearing current pulse occurs inside the bearing.
3) The two poles must have a "good" electrical connection to the outer and inner bearing race respectively.

Similar to the situation with brushes, 3) can be achieved by taking the machine end-shield and the shaft as the two poles, respectively. We will discuss more details of this aspect later (Section V-D), and first address 1) and 2).

In order to fulfill 1) and 2), a very small gap spacing and a geometry that results in local field enhancement, such as electrically conducting tips with very small diameters, would need to be provided. (Here, "very small" refers to the dimensions that drives-engineers usually deal with.) Approximating the results summarized earlier (Section IV–E) with $V_{\text{B}}/d \approx 100$ V/μm and 2 μm tip diameter, breakdowns at $\approx$2 V would require gap spacings of 0.02 μm. This is even at the very low end of the surface roughnesses that are achieved either with polishing or superfinishing [35]. Thus, it is not directly applicable here as such. However, lower V_{B}/d ratios could be achieved by exploiting the influence of the local electrical field concentration with very sharp edges, and thus, with smaller tips. Without electric field distortion by dielectric materials around the electrode tips, approximating the field enhancement factor $\beta \propto r^{-1}$, where r is the radius of the tip, $V_{\text{B}}/d \approx 1$ V/μm can be found at 0.02 μm tip diameter. Then, breakdowns at $\approx$2 V would require gap spacings of 2 μm. With typical roughnesses of approximately 1.6–6.3 μm, this is at the low end of the surface roughnesses of machine shafts. Though a surface polish could be applied to the machine shaft, this would require additional work, and the gap spacing would be difficult to maintain under normal operating conditions.

C. Solution: Conductive Microfibers

It would be very difficult—and for a commercial application probably almost impossible—to develop a system of solid metallic finger tips that could be maintained at the required distance to the shaft. However, conductive microfibers do provide a good alternative solution. These are fibers with strands less than one denier, where one denier equals 1 g per 9000 m of fiber. They are mechanically flexible and yet high strength, high-stiffness fibers.

Such conductive microfibers have very small diameters of less than 10 μm. Under the influence of an applied voltage, they emit current due to the electric field emission effect (Section IV-C) because of the locally highly enhanced electric field at the truncated fiber tips. Due to their mechanically flexible structure, if applied with the correct interference, the microfibers can maintain contact with the surface, thereby compensating the surface roughness of the shaft. In spite of the rotating movement of the shaft, the microfibers only "see" one nonrotating second pole, and the rotation of the machine shaft does not affect the functional capability of the fibers.

When a multitude of such fibers is assembled around a machine shaft, a high density of contact points is given, and many parallel paths

1) either for current to flow
2) or for a breakdown to occur

are provided.

1) When the mechanical contact is also electrically "good," current flows through the microfibers.
2) When the microfibers lose good electric contact by mechanical contact, a breakdown due to local field emission will occur somewhere along the circumference, thereby reestablishing the electric contact.

In order to fulfill 1), the microfibers must be able to carry the current that is driven by the voltage across the bearing v_{bea}. This current is mainly a function of v_{bea} and R_{f}, the resistance between the microfibers and the shaft, which is a strong function of the current. Furthermore, in order to protect the bearing, the resistance has to be so small that the voltage across the resistance does not exceed the bearing breakdown voltage. To assess the orders of magnitudes that affect the fiber design, we first approximate the current density of the fibers with 10^{10} A/m^2 (conservative estimate, using [31] as starting point). In this case, a fiber with a 1 μm tip and thus $A_{\text{c}} = 0.78 \times 10^{-12}$ m^2 cross-sectional area would be able to carry 7.8 mA. To carry a current of 7.8 A, 1000 fibers would be required. In the next step, we set the resistance R_{f} to zero. Then, the CM voltage is in parallel to the capacitance between the stator-winding and the rotor C_{wr}, as the rotor is shorted to the frame of the machine. Taking by intention (very) high values for both the dv/dt of the CM voltage, 2 kV/μs, and the value of C_{wr}, 500 nF, we obtain a current of 2 kV/μs $\times$ 500 nF $=$ 1 A. This current is almost one order of magnitude smaller than the estimated current carrying capability with as few as 1000 fibers.

The previous rough calculations illustrate that a tradeoff has to be made: properly designed fibers: 1) carry the current in parallel to the bearing and prevent voltage to build up across the bearing and 2) lead to a breakdown the moment a "good" electric contact between the fibers and the shaft is lost.

The close view of a realization of such a ring of conductive microfibers and the ring as it is mounted on a machine are shown in Figs. 6 and 7, respectively.

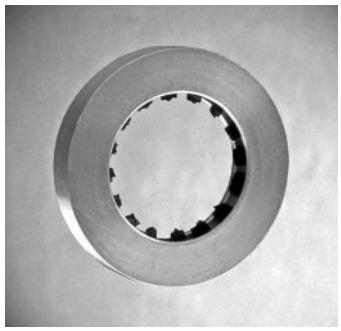

Fig. 6. Conductive microfibers assembled in rings to form static charge dissipation devices for mitigation of EDM-bearing currents.

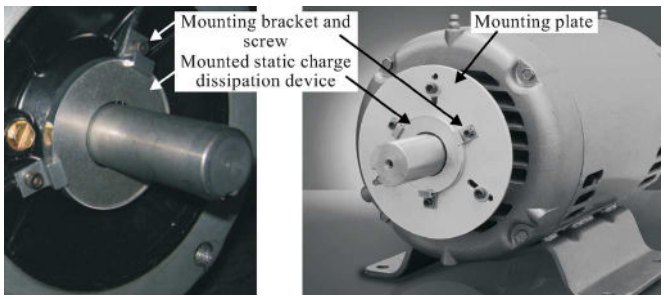

Fig. 7. Ring with conductive microfibers (static charge dissipation device) mounted at a machine shaft to obtain discharge of the voltage across the bearing through a parallel path (four-pole squirrel-cage induction motors with 1 hp rated power and 143 TC frame).

In this paper, we focus on the application of such brushes as mitigation technique for EDM-bearing currents. These currents occur predominantly with rather small motors up to several kilowatts rated power. Such brushes can also be used with larger motors for current-carrying purposes. This subject will be the topic of a different publication.

D. Comments on Robustness and Mounting

If properly designed, the interference between the fibers and the shaft can have ultralow friction, giving a technique that can be considered as free of direct frictional wear. Furthermore, the fibers can be designed to cut through contaminants such as given by oily, greasy, moist, and dusty environments. The fibers can be assembled to give a ring with a rather slim design that can be mounted on both the nondrive- and drive-end of a machine with rigid mounting plates or mounting brackets, where the electric contact is ensured with screws (Fig. 7). Thereby, no machining is required, and the installation of the device is relatively simple. In Section VI, we will report on the test results of the proposed microfiber solution. On an additional long-term test of 8700 h of operation, it was also found that the performance of the conductive microfibers was not changed. Thousands of microfiber rings have been installed in diverse applications such as paper mills, hospitals, and other heating, ventilation, and air conditioning (HVAC) fans over the last two years. Reports from the field have shown that the conductive microfiber ring is very effective and an economical solution to variable-frequency drive (VFD) related bearing failure.

TABLE III
DATA OF THE TEST DRIVES

MOTORS			
Name	Power rating	Frame	Shaft diameter
Motor MA	1HP (0.75kW)	143TC	15.9mm
Motor MB	10HP (7.5kW)	215TC	34.9mm
INVERTERS			
Name	Power rating	Carrier frequency	Control
Inverter Ia	13.7kVA	(1...12)kHz	PWM
Inverter Ib	13.7kVA	(2.5...5)kHz	PWM

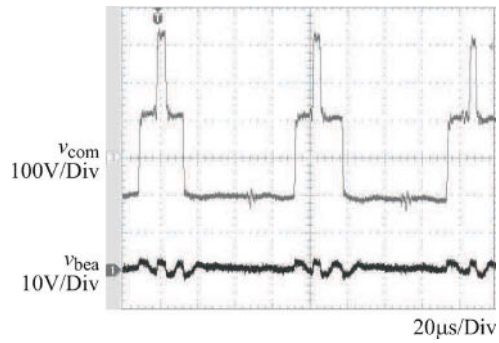

Fig. 8. CM voltage v_{com} and voltage across the bearing v_{bea} *with* ring of conductive microfibers; motor MB, 215 TC frame, 10 hp rated power, motor speed 1800 r/min, inverter Ia, carrier frequency 12 kHz, compare with Fig. 1

VI. EXPERIMENTAL RESULTS

A. Test Setup

The ability of rings of conductive microfibers to prevent a voltage of several volts to build up across the bearing was verified with a series of tests. We are reporting on selected tests that were carried out with two four-pole 50/60 Hz 230 V/460 V off-the-shelf squirrel-cage induction motors and two off-the-shelf 460 V voltage-source inverters (Table III).

For all configurations, the CM voltage v_{com} and the voltage across the bearing v_{bea} were measured during the operation, both *with* and *without* the rings of conductive microfibers being applied. This was done for different motor speed (up to two times no-load speed), additional grease ("contamination") on the motor shaft and the fibers, and variable switching frequency. Also, an additional test was carried out with the machine and the ring from microfibers being applied for 8700 h of operation. The measurements of the voltages were carried out with the help of an artificial star-point, 500 MHz voltage probes, and a 600 MHz, 5 GS/s scope.

B. Results

Fig. 8 shows the measured waveforms of v_{com} and v_{bea} of the same test setup as Fig. 1, but now a ring of conductive microfibers is applied. When comparing the two figures, it can be seen that the voltage across the bearing is reduced to a maximum of 4–7 V peak-to-peak and 4 Vp. Thus, the ring prevents the voltage across the bearing to build up to levels where the bearing

TABLE IV
OVERVIEW OF THE TESTS SHOWN IN FIGS. 1 AND 8 THROUGH 10

Test	Motor	Inverter	Speed	Brush	Other	Figure
T1N	MB	Ia	1800r/min	N		1
T1Y	MB	Ia	1800r/min	Y		8
T2N	MA	Ia	1800r/min	N		9(a)
T2Y	MA	Ia	1800r/min	Y		9(b)
T3N	MB	Ib	1800r/min	N		10(a)
T3Y	MB	Ib	1800r/min	Y		10(b)
T3G	MB	Ib	1800r/min	Y	greased*	10(c)
T3S	MB	Ib	3600r/min	Y		10(d)

* Grease is applied on the shaft and around the fibers.
Carrier frequency of inverter Ia 12kHz and of inverter Ib 2.5kHz.

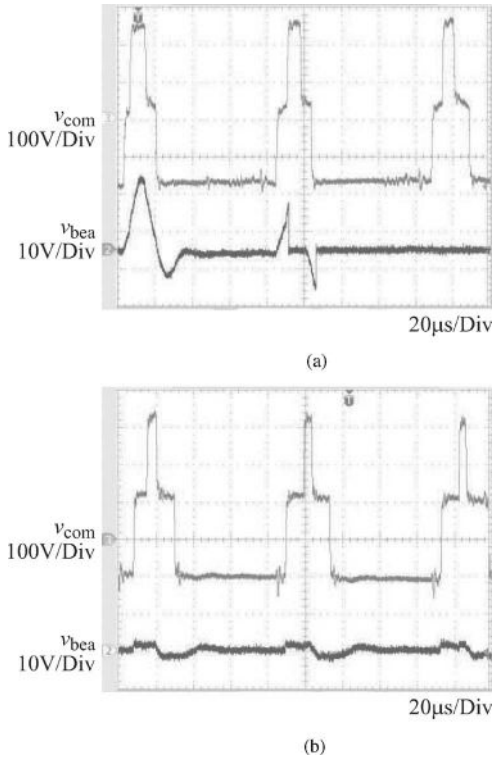

Fig. 9. CM voltage v_{com} and voltage across the bearing v_{bea}; motor MA, 143 TC frame, 1 hp rated power, motor speed 1800 r/min, inverter Ia, carrier frequency 12 kHz. (a) Without ring of conductive microfibers (test T2N). (b) With ring of conductive microfibers (test T2Y).

is endangered, as the bearing is shorted through a parallel low-resistance path.

For the various configurations discussed earlier (Section VI-A), voltage build-up across the bearing and subsequent breakdown could be observed when no additional device was applied. However, with a ring of conductive microfibers being applied, the voltage was reduced to a maximum of 4–7 V peak-to-peak and 4 Vp, and no breakdown events were observed. With respect to the additional long-term test, the amount of wear was too negligible to alter the performance.

For illustration, the measured traces of v_{com} and v_{bea} for selected configurations from the series of measurements are shown in Figs. 8 through 10, where Figs. 9(a) and 10(a) show the

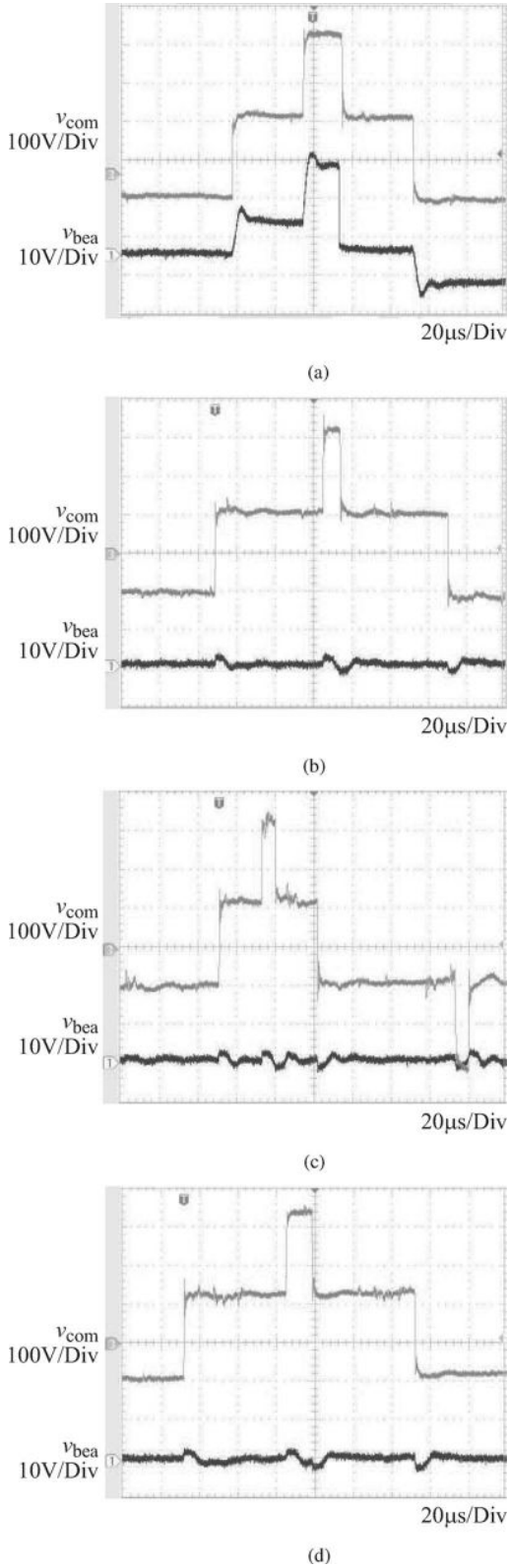

Fig. 10. CM voltage v_{com} and voltage across the bearing v_{bea}; motor MB, 215 TC frame, 10 hp rated power, motor speed 1800 r/min unless otherwise stated, inverter Ib, 2.5 kHz carrier frequency. (Note: When comparing with Figs. 1, 8, and 9, the lower carrier frequency of the second inverter is also clearly to see.) (a) Without ring of conductive microfibers (test T3N). (b) With ring of conductive microfibers (test T3Y). (c) With ring of conductive microfibers, grease applied on the shaft (test T3G). (d) *With* ring of conductive microfibers, motor speed 3600 r/min (test T3S).

measurement results when no additional device was applied, and Figs. 8, 9(b), and 10(b)–(d) show measurement results with a ring of conductive microfibers being applied. More details of the individual configurations are shown in Table IV.

These pictures illustrate well the corrective effect of the ring of conductive microfibers on the voltage build-up across the bearing and the subsequent breakdown phenomena, thereby confirming the ability of this device to serve as an effective mitigation technique for electric discharge bearing currents.

VII. Conclusion

A new mitigation technique for EDM-bearing currents that uses static charge dissipation has been presented. With this technique, the voltage across the bearing is discharged at very low levels and before an electric breakdown inside the bearing occurs. The technique is based on the field emission effect, has ultralow friction and negligible wear, and is very robust toward contamination, when compared to conventional carbon-based brushes. With this technique, a high density of contact points given by a multitude of conductive microfibers that are arranged in parallel to the bearing via a supporting ring is used to provide many parallel paths for current to flow or a breakdown to occur outside of the bearing. It was shown that it is important to include the electric field emission effect in the theoretical analysis of the orders of magnitudes of the parameters that are involved in the design process. Furthermore, a series of measurement results that confirms the effectiveness of the proposed mitigation technique for EDM-bearing currents was presented.

References

[1] S. Chen, T. A. Lipo, and D. Fitzgerald, "Modelling of motor bearing currents in inverter drives," *IEEE Trans. Ind. Appl.*, vol. 32, no. 6, pp. 1365–1370, Nov./Dec. 1996.

[2] J. Erdman, R. Kerkman, and D. Schlegel, "Effect of PWM inverters on AC motor bearing currents and shaft voltages," *IEEE Trans. Ind. Appl.*, vol. 32, no. 2, pp. 250–259, Mar./Apr. 1996.

[3] D. Busse, J. Erdman, R. Kerkman, D. Schlegel, and G. Skibinski, "The effect of PWM voltage source inverters on the mechanical performance of rolling bearings," *IEEE Trans. Ind. Appl.*, vol. 33, no. 2, pp. 567–576, Mar./Apr. 1997.

[4] D. Busse, J. Erdman, R. Kerkman, and D. Schlegel, "Bearing currents and their relationship to PWM drives," *IEEE Trans. Power Electron.*, vol. 12, no. 2, pp. 243–252, Mar. 1997.

[5] D. Busse, J. Erdman, R. Kerkman, D. Schlegel, and G. Skibinski, "System electrical parameters and their influence effect on bearing currents," *IEEE Trans. Ind. Appl.*, vol. 33, no. 2, pp. 577–584, Mar./Apr. 1997.

[6] D. Busse, J. Erdman, R. Kerkman, D. Schlegel, and G. Skibinski, "Characteristics of shaft voltage and bearing currents," *IEEE Ind. Appl. Mag.*, vol. 3, no. 6, pp. 21–32, Nov./Dec. 1997.

[7] A. von Jouanne, H. Zhang, and A. K. Wallace, "An evaluation of mitigation techniques for bearing currents, EMI and overvoltages in ASD applications," *IEEE Trans. Ind. Appl.*, vol. 34, no. 5, pp. 1113–1122, Sep./Oct. 1998.

[8] P. Link, "Minimizing electric bearing currents in ASD systems," *IEEE Ind. Appl. Mag.*, vol. 5, no. 4, pp. 55–66, Jul./Aug. 1999.

[9] A. Binder, R. Aust, and A. Schrepfer, "Bearing currents—A danger to inverter-fed AC-motors?," *Iron Steel Eng.*, vol. 76, no. 7, pp. 47–52, Jul. 1999.

[10] S. Bell, T. J. Cookson, S. A. Cope, R. A. Epperly, A. Fischer, D. W. Schlegel, and G. L. Skibinski, "Experience with variable-frequency drives and motor bearing reliability," *IEEE Trans. Ind. Appl.*, vol. 37, no. 5, pp. 1438–1446, Sep./Oct. 2001.

[11] H. E. Boyanton and G. Hodges, "Bearing fluting," *IEEE Ind. Appl. Mag.*, vol. 8, no. 5, pp. 53–57, Sep./Oct. 2002.

[12] R. Naik, T. A. Nondahl, M. J. Melfi, R. F. Schiferl, and J. S. Wang, "Circuit model for shaft voltage prediction in induction motors fed by PWM-based AC drives," *IEEE Trans. Ind. Appl.*, vol. 39, no. 5, pp. 1294–1299, Sep./Oct. 2003.

[13] R. F. Schiferl and M. J. Melfi, "Bearing current remediation options," *IEEE Ind. Appl. Mag.*, vol. 10, no. 4, pp. 40–50, Jul./Aug. 2004.

[14] A. Muetze, *Bearing Currents in Inverter-Fed AC Motors*. Aachen, Germany, Shaker Verlag, 2004..

[15] A. Muetze and A. Binder, "Don't lose your bearings—Mitigation techniques for bearing currents in inverter-supplied drive systems," *IEEE Ind. Appl. Mag.*, vol. 12, no. 4, pp. 22–31, Jul./Aug. 2006.

[16] A. Muetze and A. Binder, "Calculation of motor capacitances for prediction of discharge bearing currents in machines of inverter-based drive systems," in *Proc. 5th IEEE Int. Electric Mach. Drives Conf. (IEMDC)*, San Antonio, TX, May, 15–18, 2005, pp. 264–270.

[17] A. E. Seaver, "An equation for charge decay valid in both conductors and insulators," in *Proc. Electrostat. Soc. Amer. Inst. Electrostat.-Jpn. (ESA-IEJ) Joint Meeting*, Chicago, IL, June 2002, pp. 349–360.

[18] M. D. Bryant, "Tribology issues in electric contacts," Lecture Notes ME 383S. Austin, TX: Lubrication, Wear and Bearing Technology, Univ. of Texas at Austin, 2006.

[19] F. Paschen, "On sparking over in air, hydrogen, carbon dioxide under the potentials corresponding to various pressures," *Wiedemann Ann. Phys. Chem.*, vol. 37, pp. 69–96, 1889.

[20] J. M. Meek and J. D. Craggs, *Electrical Breakdown of Gases*. New York: Wiley, 1978.

[21] H. Raether, *Electron Avalanches and Breakdown in Gases*. London,, U.K.: Butterworth, 1964.

[22] I. Gallimberti, "The mechanism of the long spark formation," *J. Phys.*, vol. 40 no. C7, pp. 193–250, Jul. 1979.

[23] E. M. Bazelyan and Y. P. Raizer, *Spark Discharge*. Boca Raton, FL: CRC Press, 1997.

[24] A. Wallash, "Electric breakdown and ESD phenomena for devices with nanometer-to-micron gaps," in *Proc. Int. Soc. Opt. Eng., Conf. Rel., Testing, Charact. MEMS/MOEMS II*, vol. 4980, no. 16, pp. 87–98, Jan. 2003.

[25] R. M. Schaffert, *Electrophotography*. New York: Wiley, 1975.

[26] A. Wallash and T. Hughbanks, "Capacitive coupling effects in spark gap devices," in *Proc. 16th Electr. Overstress Discharge (EOS/ESD) Symp.,* EOS/ESD Assoc., pp. 273–278, 1994.

[27] R. H. Fowler and L. Nordheim, "Elecron emission in intense electric fields," in *Proc. Royal Soc. London, Ser. A, Containing Pap. Math. Phys. Charact.*, vol. 119, no. 781, pp. 173–181, May 1928.

[28] T. E. Stern, B. S. Gossling, and R. H. Fowler, "Further studies in the emission of electrons from cold metals," in *Proc. Royal Soc. London, Ser. A, Containing Pap. Math. Phys. Charact.*, vol. 124, no. 795, pp. 699–723, Jul. 1929.

[29] F. Gomer, *Field Emission and Field Ionization*. Cambridge, MA: Harvard Univ. Press, 1961.

[30] C. A. Spindt, I. Brodie, L. Humphrey, and E. R. Westerberg, "Physical properties of thin-film field emission cathodes with molybdenum cones," *J. Appl. Phys.*, vol. 47, no. 12, pp. 5248–5263, Dec. 1976.

[31] P. G. Slade and E. D. Taylor, "Electrical breakdown in atmospheric air between closely spaced (0.2 μm–40 μm) electrical contacts," *IEEE Trans. Compon. Packag. Technol.*, vol. 25, no. 3, pp. 390–396, Sep. 2002.

[32] A. Wallash and L. Levit. (Jan. 2003), "Electrical breakdown and ESD phenomena for devices with nanometer-to-micron gaps" in presentation at Int. Soc. Opt. Eng., Conf. Rel., Testing, Charact. MEMS/MOEMS [Online]. Available: http://www.wallash.com/allpubs.htm.

[33] R. T. Lee, H. H. Chung, and Y. C. Chiou, "Arc erosion of silver electric contacts in a single arc discharge across a static gap," in *Proc. IEE Sci., Meas. Technol.*, vol. 148, no. 1, pp. 8–14, Jan. 2001.

[34] J. M. Torres and R. S. Dhariwal, "Electrical field breakdown at micrometre separations," *Nanotechnology*, vol. 10, no. 1, pp. 102–107, Mar. 1999.

[35] *Guide to the Selection of The Surface Finish of Stainless Steel on Fabricated Items,* Solids Handling Process. Assoc. (SHAPA) Tech. Bull., 1, Jan. 2000.

Annette Muetze (S'03–M'04) received the Dipl.-Ing. degree in electrical engineering from Darmstadt University of Technology, Darmstadt, Germany and the degree in general engineering from the Ecole Centrale de Lyon, Ecully, France, both in 1999, and the Dr. Tech. degree in electrical engineering from Darmstadt University of Technology in 2004.

During 2004, she was an Assistant Professor at the Electrical and Computer Engineering Department, University of Wisconsin-Madison, Madison. Since January 2007, she has been a Lecturer in the School of Engineering, University of Warwick, Coventry, UK.

Dr. Muetze was the recipient of the FAG Innovation Award 2004 for her work on inverter-induced bearing currents. She was also the recipient of the National Science Foundation CAREER Award in 2005.

H. William Oh (M'03) received the B.Sc. degree from Pusan National University, Pusan, Korea, in 1982, and the M.Sc. degree from Korea Advanced Institute of Science and Technology, Seoul, Korea, 1984, both in mechanical engineering.

From 1985 to 1988, he was with the University of Massachusetts, Amherst. He is currently the General Manager of Electro Static Technology, a division of Illinois Tool Works (ITW), Mechanic Falls, ME. He is the inventor of the AEGIS SGR Shaft Grounding Ring manufactured by Electro Static Technology. He has extensive design and application experience in rotating shaft grounding and sliding electrical contacts, specializing in the mitigation of unwanted electrical currents. He is the holder of eight patents.

Mr. Oh is a member of the Illinois Tool Works Patent Society.